Supporting Information

Ionic Self-Assembly of Pillar[5]arenes: Proton-Conductive Liquid Crystals and Aqueous Nanoobjects with Encapsulation Properties

Iván Marín,[a,b] Rosa I. Merino,[a,c] Joaquín Barberá,[a,b] Alberto Concellón,[a,b] and José L. Serrano[a,b,]*

a. Instituto de Nanociencia y Materiales de Aragón (INMA), CSIC-Universidad de Zaragoza, 50009 Zaragoza, Spain.

b. Departamento de Química Orgánica, Facultad de Ciencias, Universidad de Zaragoza, 50009 Zaragoza, Spain.

c. Departamento de Física de la Materia Condensada, Facultad de Ciencias, Universidad de Zaragoza, 50009 Zaragoza, Spain.

Author for correspondence: joseluis@unizar.es

Table of Contents

1. MATERIALS AND CHARACTERIZATION TECHNIQUES

All reagents were purchased from Aldrich and used without further purification. Anhydrous CH_2Cl_2 and THF were purchased from Scharlab and dried by using a solvent purification system. ^1H NMR and ^{13}C NMR spectra were acquired on a Bruker AV400 spectrometer. The experiments were performed at room temperature in different deuterated solvents ($CDCl_3$ CD_2Cl_2 or DMSO-d_6). Chemical shifts are given in ppm relative to TMS and the solvent residual peak was used as the internal standard. Infrared spectra were recorded on a Bruker Vertex 70 FT-IR spectrometer. The samples were prepared on KBr pellets with a concentration of the product of 1-2% (w/w). Mass spectra were obtained on a MICROFLEX Bruker (MALDI+) spectrometer with a dithranol matrix.Mesogenic behavior was investigated by polarized-light optical microscopy (POM) using an Olympus BH-2 polarizing microscope fitted with a Linkam THMS600 hot stage. Thermogravimetric analysis (TGA) was performed using a Q5000IR from TA instruments at heating rate of 10 °C min^{-1} under a nitrogen atmosphere. Thermal transitions were determined by differential scanning calorimetry (DSC) using a DSC Q2000 from TA instruments with powdered samples (2–5 mg) sealed in aluminum pans. Glass transition temperatures (Tg) were determined at the half height of the baseline jump, and first order transition temperatures were read at the maximum of the corresponding peak.

UV-Vis absorption spectra were recorded on an ATI-Unicam UV4-200 spectrophotometer. Fluorescence measurements were performed using a Perkin-Elmer LS 50B fluorescence spectrophotometer.

X-ray diffraction measurements were carried out using an XRD-PANanalytical Empyrean diffractometer equipped with platform Scatter X78. Samples were heated until isotrope temperature between two kapton films then were allowed to cold down untill room temperature. Photographic patterns were recorded with a Pinhole camera (Anton Paar) operating with a point-focused Ni-filtered Cu-Kα beam. Samples were contained in Lindemann glass capillaries (0.9 or 0.7 mm diameter) and, when necessary, a variable-temperature attachment was used to heat the sample. The patterns were collected on flat photographic film perpendicular to the X-ray beam.

Electrochemical impedance spectroscopy was recorded with a SI1260 Frequency Response Analyser from Schlumberger Instruments in the frequency range from 1 Hz to 1 MHz, with an AC applied voltage 50 mV amplitude. The sample with ITO coated glass slides and spacers was placed inside a variable temperature hotstage equipped with a temperature controller (Linkam TMS94). The conductivities were studied as a function of temperature between 30°C and isotrope temperature at 5°C intervals. For the preparation of the cells, the appropriate amount of the ionic dendrimer was placed onto an ITO electrode that was sandwiched with another ITO electrode controlling the thickness by using glass spacers (25 µm). The cell was heated up to a few degrees above the melting point of the liquid crystal and the cell was pressed to obtain the thin film. The impedance spectrum was analysed using Nyquist plots, imaginary (Z'') versus real (Z') components, see figures S25. The resistance (R_b) was estimated from the

intersection of the real axis (Z') and the high frequency semicircle of the impedance spectrum. Alternatively, R_b was taken from the Z' value at the minimum between the high frequency semicircle and low frequency spike. The conductivities σ (S·cm^{-1}) were calculated with the formula: $\sigma = d / (R_b \cdot A)$), where d (cm) is the thickness of the film, A (cm^2) is the area of the film and R_b (Ω) is the resistance of the sample.

After the preparation of the cell, a random orientation of the mesophase was observed between electrodes. Nematic samples were mechanically sheared within the cell (in order to obtain an alignment of the molecules) at isotropic temperature and then slowly cool down to room temperature (0.05 ºC·min^{-1}).

Photocrosslinking of coumarin units (photodimerization) was carried out by exposing the aligned LC films of 25 μm of thickness to 325 nm LED light (ThorsLab) for 60 min with a UV power of 8 mW/cm^2.

Microscopy (TEM) analysis was performed using a FEI Tecnai T20 microscope (FEI Company, Waltham, MA, USA) operating at 200 kV. TEM samples were prepared adding 10 μL of each self-assembly dispersion at an approximately 1.0 mg mL^{-1} concentration on a continuous carbon film-copper grid, and the excess was removed by capillarity using filter paper. Then, the grids were stained with uranyl acetate (1% aqueous solution), removing the excess again by capillarity using filter paper.

2. EXPERIMENTAL PROCEDURES

2.1 General procedure for the preparation of ionic complexes

The synthesis of the different acids and pillararene **P5N10** was carried out following antecedent papers[i,ii,iii]. Ionic dendrimers were prepared following the previously described methodology[iv]. A solution of corresponding acid in dry tetrahydrofuran was added to a solution of the pillararene **P5N10**, in approximately 1:1 (primary amine groups: carboxylic acid groups) stoichiometry. The mixture was ultrasonicated for 5 min, and then it was slowly evaporated at room temperature and dried in vacuum at 40ºC until the weight remained constant.

AcC$_{11}$-P5N10. IR (KBr, ν, cm^{-1}): 3423 (-NH$_3$$^+$), 2949 (=C-H), 2925 (C-H), 1652 (C=O), 1636 (Ar), 1558 (COO$^-$asym), 1406 (COO$^-$sym), 1217 (C-O). ^{1}H NMR (CDCl$_3$, 298K, 400 MHz, δ, ppm): 6.80 (s, 10H), 5.87 (s, 40H), 4.11 (m, 20H), 3.70 (s, 10H), 3.20 (m, 20H), 2.23 (t, J=10 Hz, 20H), 1.57 (q, J=8.52 Hz, 20H), 1.24 (m, 130H), 0.87 (t, J=9.2 Hz, 30H). ^{13}C NMR (CDCl$_3$, 298K, 100 MHz, δ, ppm): 180.38, 150.19, 129.55, 116.53, 67.62, 39.65, 36.83, 32.08, 29.83, 29.53, 26.13, 22.84, 14.25.

AcBzC$_{11}$-P5N10. IR (KBr, ν, cm^{-1}): 3440 (-NH$_3$$^+$), 2918 (=C-H), 2852 (C-H), 1689 (C=O), 1607 (Ar), 1539 (COO$^-$asym), 1380 (COO$^-$sym), 1205 (C-O). ^{1}H NMR (CDCl$_3$, 298K, 400 MHz, δ, ppm): 7.91 (d, J=8.08 Hz, 20H), 6.82 (s, 10H), 6.72 (d, J=8.08Hz, 20H), 5.07 (s, 30H), 3.85 (m, 20H), 3.09 (s, 30H), 1.73 (m, 20H), 1.30 (m, 160H), 0.88 (t, J=7.04 Hz, 30H). ^{13}C NMR (CDCl$_3$, 298K, 100 MHz, δ, ppm): 172.78, 162.05, 150.41, 131.61, 129.55, 126.66, 115.52, 113.83, 68.16, 39.48, 32.06, 29.76, 29.64, 29.49, 29.41, 26.21, 22.83, 14.26.

Acd$_1$C$_{11}$-P5N10. IR (KBr, v, cm^{-1}): 3327 (-NH$_3$$^+$), 2940 (=C-H), 2848 (C-H), 1712 (C=O), 1620 (Ar), 1512 (COO$^-$asym), 1434 (COO$^-$sym), 1296 (C-O).^{1}H NMR (CDCl$_3$, 298K, 400 MHz, δ, ppm): 7.25 (s, 20H), 6.84 (s, 10H), 3.97 (m, 60H), 3.70 (m, 80H), 1.73 (hex, J=6.96 Hz, 60H), 1.43 (hex, J=6.96Hz, 60H), 1.25 (m, 420H) 0.87 (t, J=6.92 Hz, 90H).^{13}C NMR (DMSO- d$_6$, 298K, 100 MHz, δ, ppm): 167.25, 140.64, 107.78, 73.14, 68.73, 31.88, 30.41, 29.72, 29.29, 26.41, 22.54.

AcC$_{11}$Cou-P5N10. IR (KBr, v, cm^{-1}): 3134 (-NH$_3$$^+$), 2925 (=C-H), 2851 (C-H), 1724 (C=O), 1617 (Ar), 1519 (COO$^-$asym), 1426 (COO$^-$sym), 1207 (C-O).^{1}H NMR (DMSO-d$_6$, 298K, 400 MHz, δ, ppm): 7.98 (d, J=9.48 Hz, 10H), 7.61 (d, J=8.6Hz, 10H), 6.95 (m, 20H), 6.82 (s, 10H), 6.28 (d, J=9.48 Hz, 10H), 4.06 (t, J=6.51 Hz, 20H), 3.75 (m, 30H), 2.95 (s, 10H), 2.17 (t, J=7.32 Hz, 20H), 1.73 (m, 20H), 1.33 (m, 140H).^{13}C NMR (DMSO-d$_6$, 298K, 100 MHz, δ, ppm): 174.55, 161.90, 160.33, 155.43, 150.94, 144.37, 134.59, 129.48, 116.66, 112.74, 112.37, 112.23, 101.12, 68.29, 59.96, 41.26, 33.73, 28.94, 28.86, 28.74, 28.70, 28.57, 28.43, 25.42, 24.33.

AcBzC$_{11}$Cou-P5N10. IR (KBr, v, cm^{-1}): 3437 (-NH$_3$$^+$), 2927 (=C-H), 2852 (C-H), 1731 (C=O), 1610 (Ar), 1558 (COO$^-$asym), 1387 (COO$^-$sym), 1206 (C-O).^{1}H NMR (CDCl$_3$, 298K, 400 MHz, δ, ppm): 7.97 (d, J=9.48 Hz, 10H), 7.85 (d, J=8.76 Hz, 20H), 7.60 (d, J=8.6Hz, 10H), 6.94 (m, 40H), 6.83 (s, 10H), 6.27 (d, J=9.48 Hz, 10H), 4.06 (t, J=6.48 Hz, 20H), 3.99 (t, J=6.48 Hz, 20H), 3.91 (s, 20H), 3.74 (s, 10H), 3.03 (s, 20H), 1.72 (m, 40H), 1.33 (m, 140H).^{13}C NMR (DMSO- d$_6$, 298K, 100 MHz, δ, ppm): 167.51, 161.90, 161.86, 160.32, 155.43, 151.17, 144.35, 131.21, 131.14, 129.47, 124.23, 113.98, 113.88, 112.72, 112.36, 112.23, 101.11, 71.25, 68.27, 67.67, 43.40, 30.70, 28.95, 28.90, 28.73, 28.69, 28.55, 28.41, 25.44, 25.40.

Acd$_1$C$_{11}$Cou-P5N10. IR (KBr, v, cm^{-1}): 3442 (-NH$_3$$^+$), 2923 (=C-H), 2848 (C-H), 1736 (C=O), 1617 (Ar), 1555 (COO$^-$asym), 1369 (COO$^-$sym), 1273 (C-O).^{1}H NMR (CDCl$_3$, 298K, 400 MHz, δ, ppm): 7.60 (d, J=9.48 Hz, 30H), 7.33 (d, J=8.6 Hz, 30H), 7.27 (s, 10H), 6.77 (m, 60H), 6.21 (d, J=9.44 Hz, 30H), 3.97 (m, 120H), 1.77 (m, 120H), 1.43 (m, 120H), 1.29 (m, 340H).^{13}C NMR (CDCl$_3$, 298K, 100 MHz, δ, ppm): 170.53, 162.48, 161.33, 143.18, 143.54, 128.67, 112.83, 112.79, 112.23, 108.50, 101.11, 73.51, 68.68, 29.82, 29.60, 29.49, 29.31, 29.21, 26.12, 26.04.

General Procedure for the preparation of the aggregates. For the preparation of the self-assemblies, a solution of 5 mg/mL of the amphiphilic ionic pillararene in THF was prepared, and Milli-Q water was gradually added while self-assembly was followed by measuring the turbidity in UV. When a critical water content was reached, a high increase in turbidity happened, indicating that the self-assembling process took place. Once turbidity reached an almost constant value, the mixture was dialyzed against water to remove the organic solvent using a Spectra/Por dialysis membrane (MWCO 1000) for 3 days. Water suspensions of the aggregates with a concentration around 2 mg/mL were obtained. Nile Red encapsulation: 119 µL of a solution of Nile Red in DCM (5×10^{-6} M) was added into flasks and then the solvent evaporated. Afterwards, a water suspension of nanoparticles of concentration 2.0 mg/mL was added to the flask. The vesicles suspensions were prepared by diluting the former 2 mg/mL nanoparticle suspension. In

each flask a final concentration of 1.0×10^{-6} M of Nile Red was reached. These solutions were stirred overnight to reach equilibrium before fluorescence was measured. The emission spectra of Nile Red were registered from 560 to 700 nm while exciting at 550 nm.
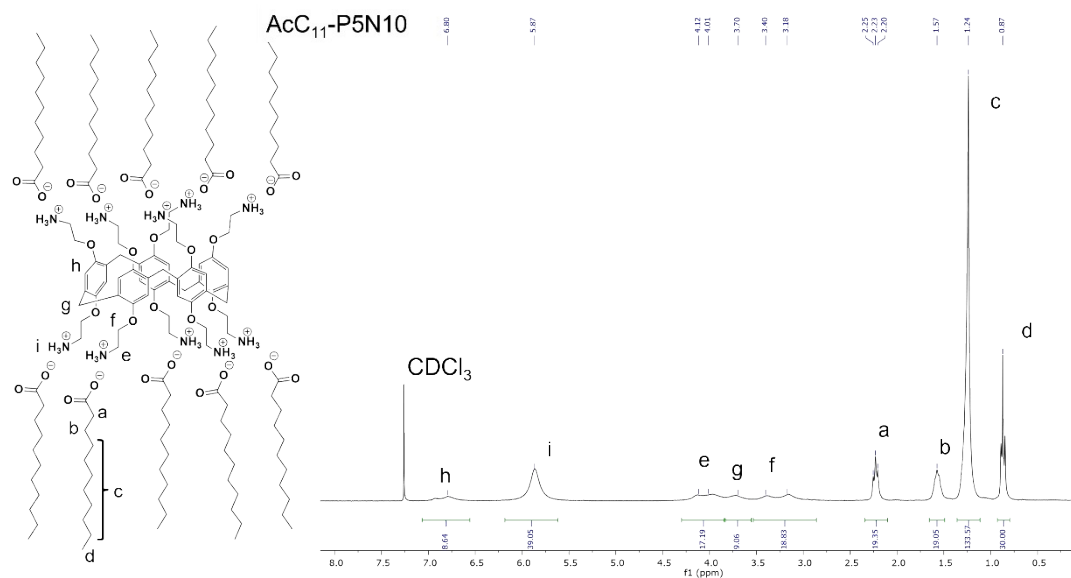
3. SUPPLEMENTARY FIGURES

3.1 NMR Spectra

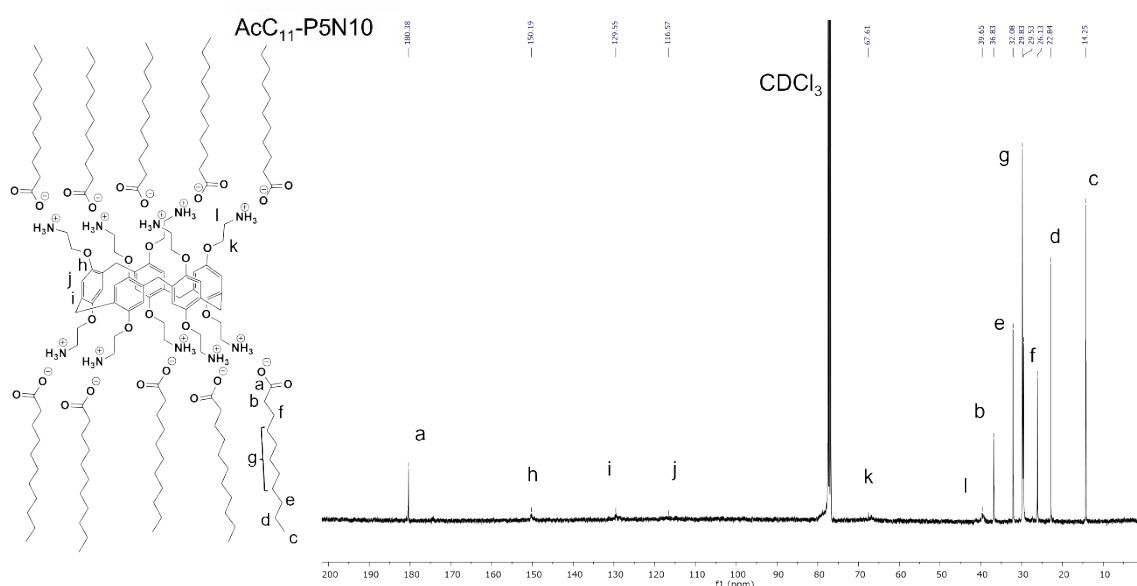Figure S1. H-NMR spectrum of AcC$_{11}$-P5N10 CDCl$_3$, 298K, 400 MHz.

Figure S2. C-NMR spectrum of AcC$_{11}$-P5N10 CDCl$_3$, 298K, 100 MHz.
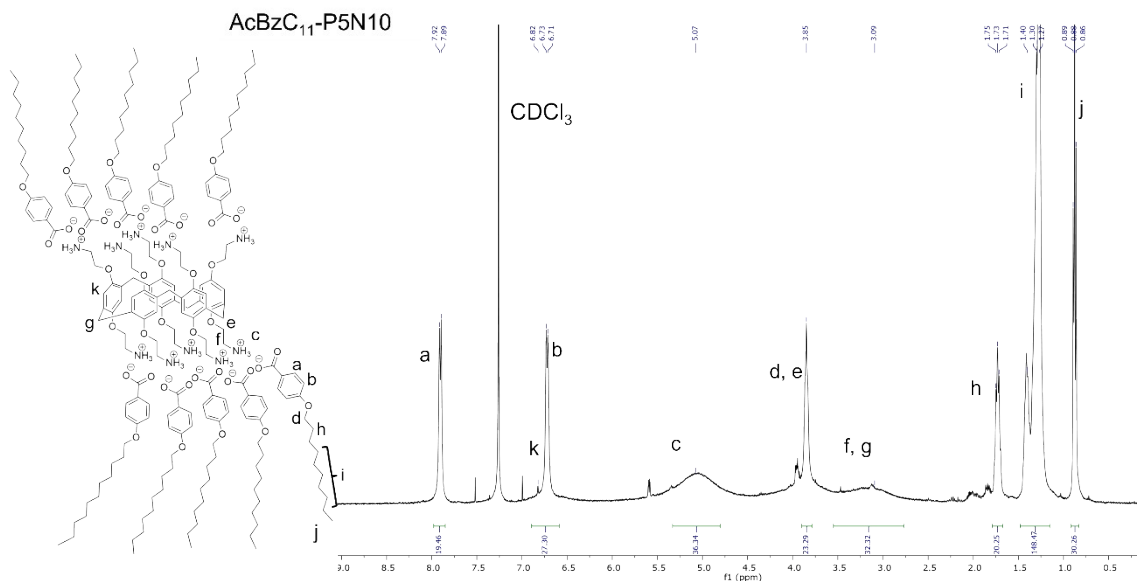
AcBzC₁₁-P5N10

Figure S3. H-NMR spectrum of AcBzC$_{11}$-P5N10 CDCl$_3$, 298K, 400 MHz.
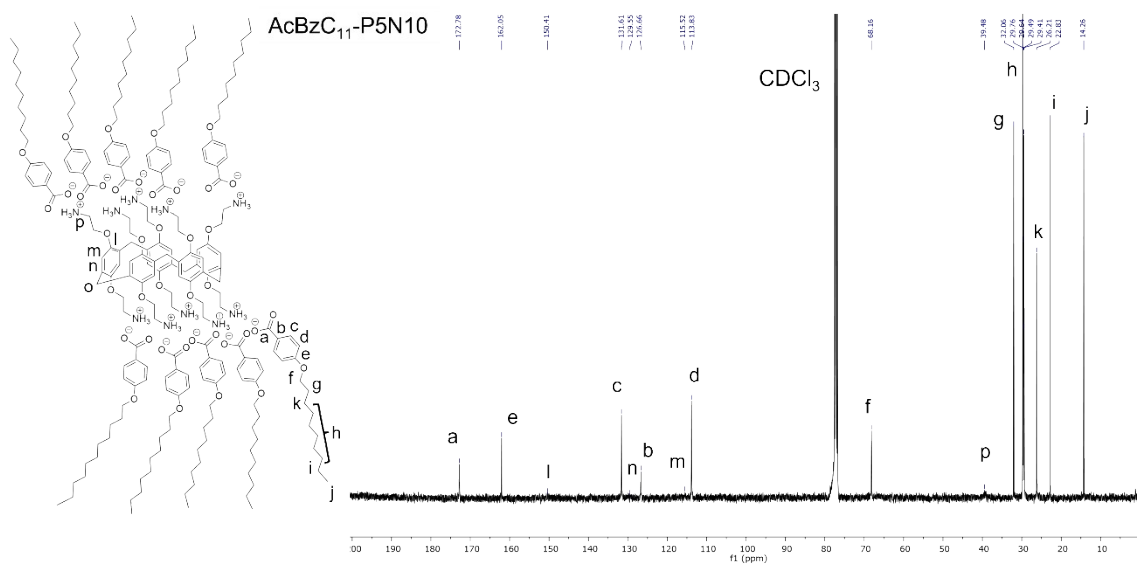
AcBzC₁₁-P5N10

Figure S4. C-NMR spectrum of AcBzC$_{11}$-P5N10 CDCl$_3$, 298K, 100 MHz.
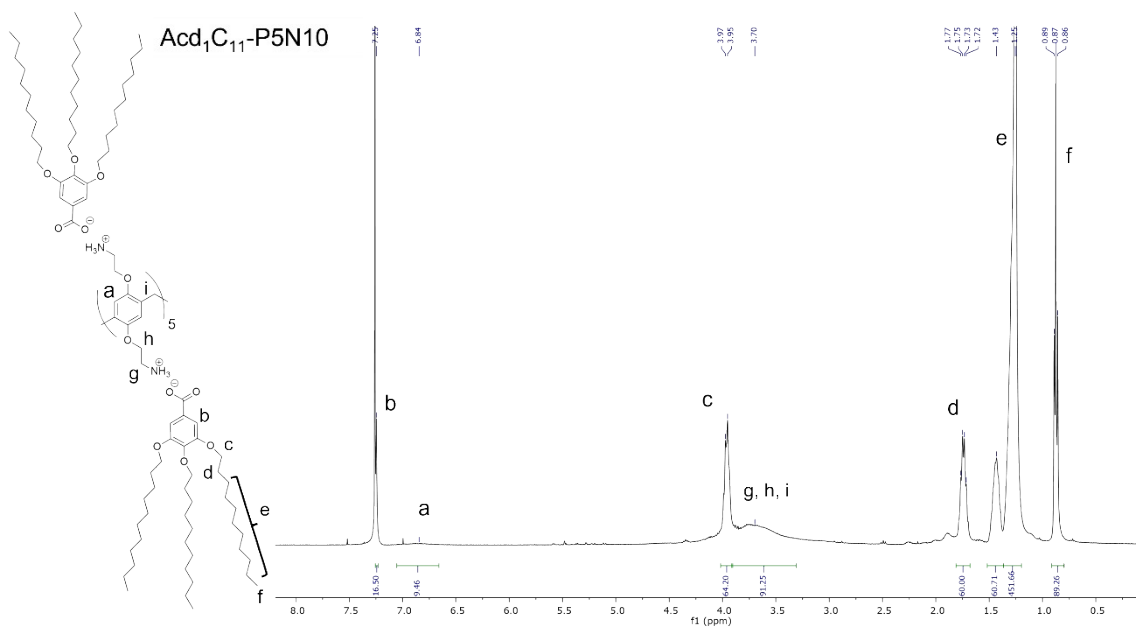
Figure S5. H-NMR spectrum Acd₁C₁₁-P5N10 CDCl₃, 298K, 400 MHz.
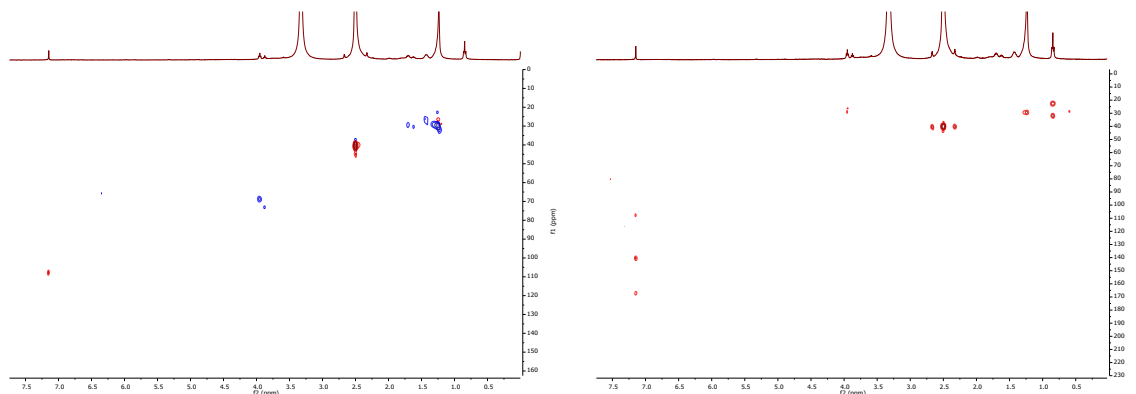
Figure S6. HSQC and HMBC spectra of Acd₁C₁₁-P5N10 CDCl₃, 298K.

Figure S7. H-NMR spectrum of AcC₁₁Cou-P5N10 DMSO-d₆, 298K, 400 MHz.

AcC₁₁Cou-P5N10

Figure S8. C-NMR spectrum of AcC₁₁Cou-P5N10 DMSO-d₆, 298K, 100 MHz.
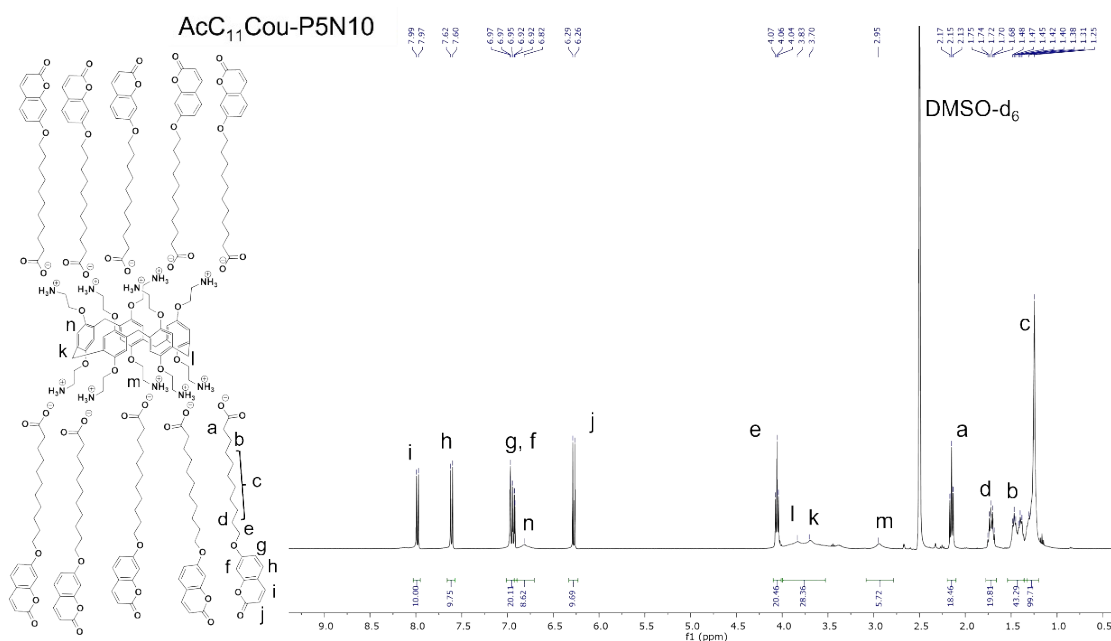
AcBzC₁₁Cou-P5N10

Figure S9. H-NMR spectrum of AcBzC₁₁Cou-P5N10 DMSO-d₆, 298K, 400 MHz.
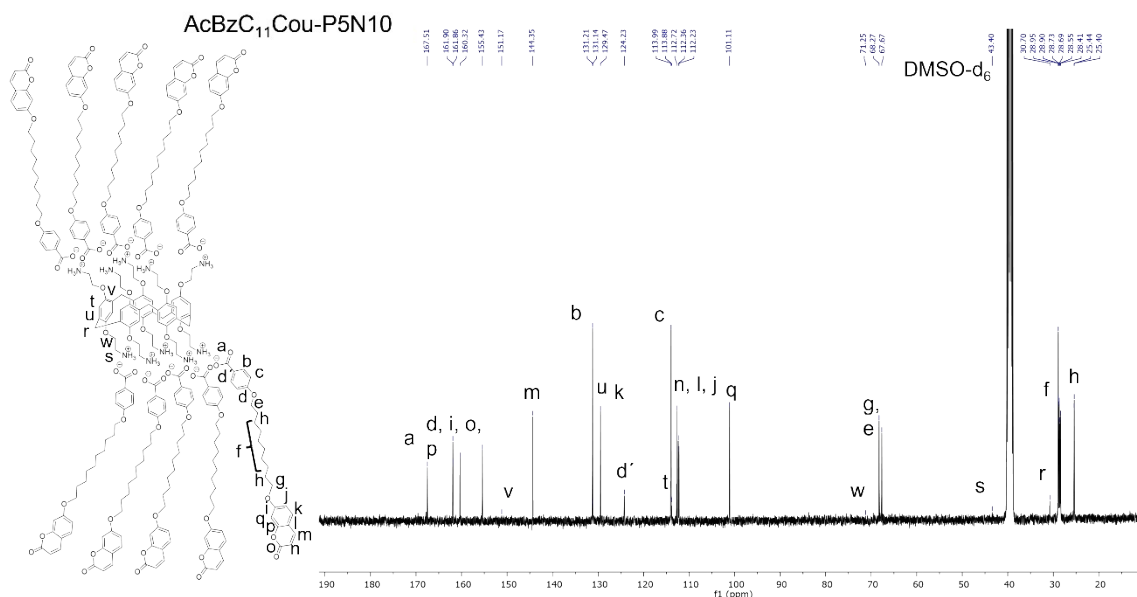
Figure S10. C-NMR spectrum of AcBzC$_{11}$Cou-P5N10 DMSO-d$_6$, 298K, 100 MHz.
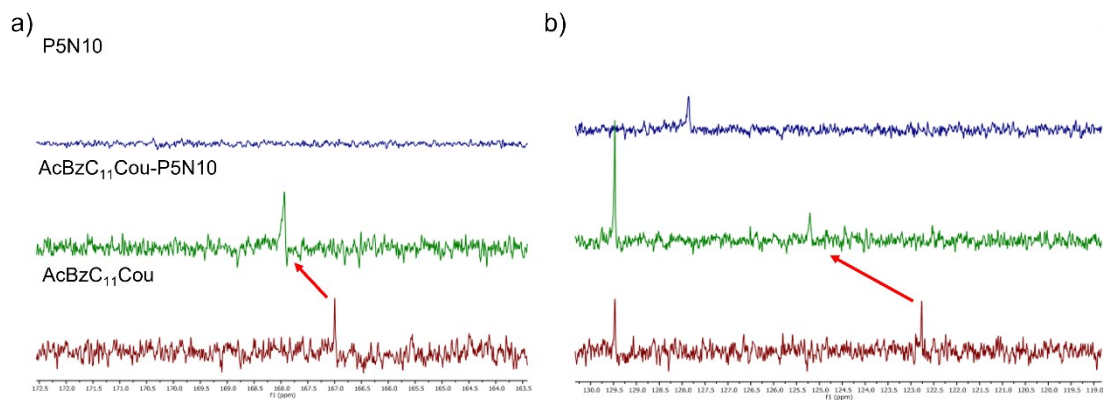
Figure S11. C-NMR comparation of P5N10, AcBzC$_{11}$Cou-P5N10 and AcBzC$_{11}$Cou DMSO-d6, 298K, 100 MHz.
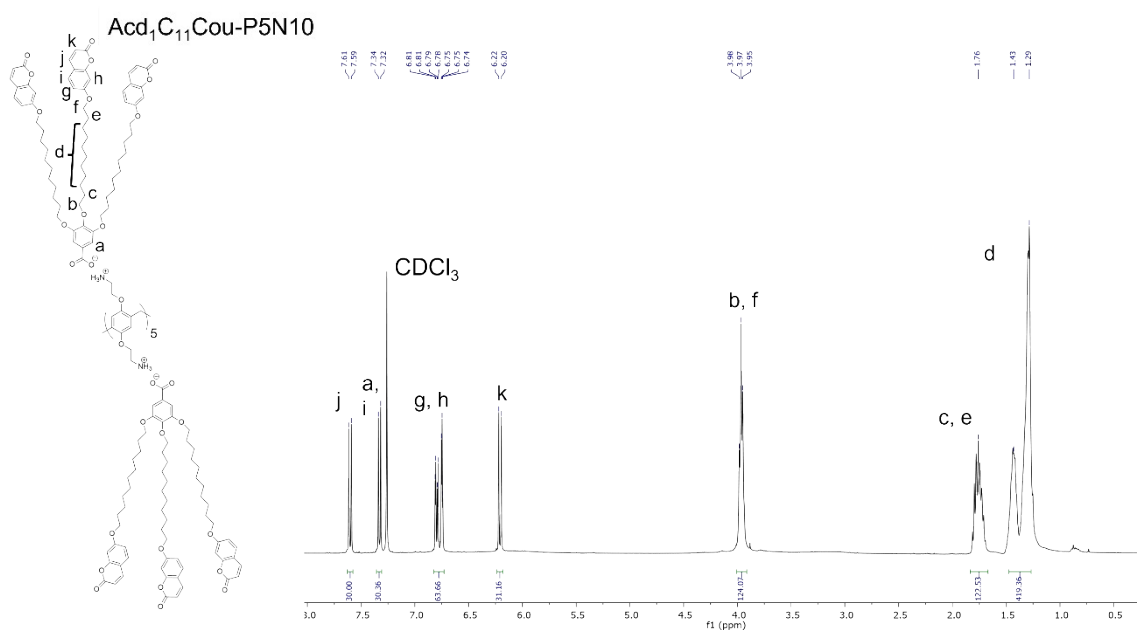
Figure S12. H-NMR spectrum of Acd$_1$C$_{11}$Cou-P5N10 CDCl$_3$, 298K, 400 MHz.
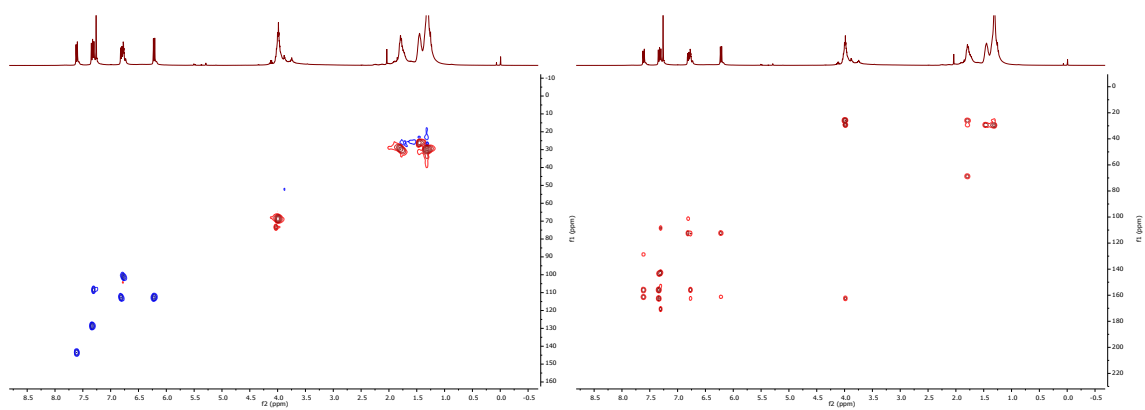
Figure S13. HSQC and HMBC spectra of Acd₁C₁₁Cou-P5N10 CDCl₃, 298K.
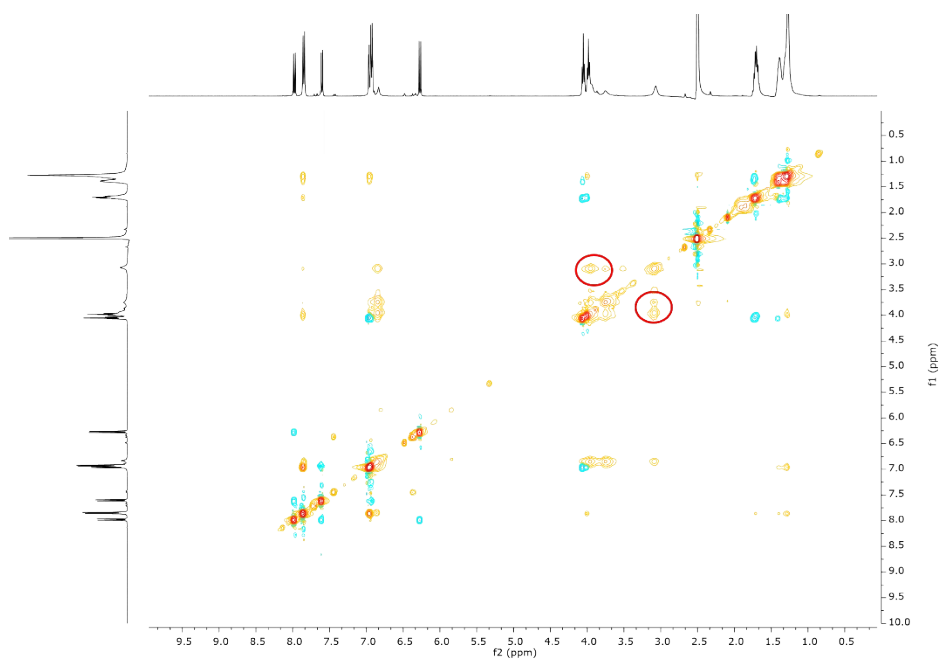
Figure S14. ¹H-¹H NOESY spectrum of AcBzC₁₁Cou-P5N10 CDCl₃, 298K.

3.2 IR spectra
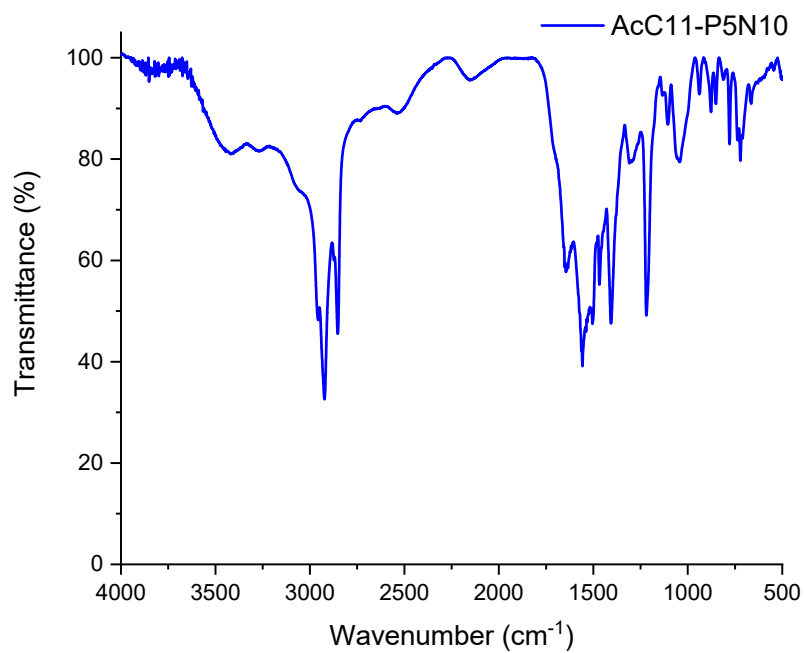
Figure S15. IR spectrum of AcC$_{11}$-P5N10
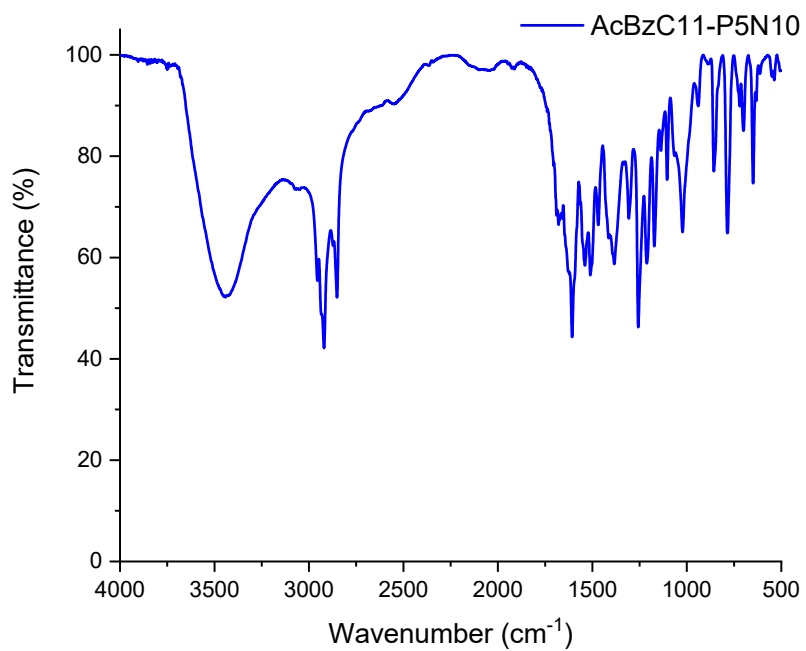
Figure S16. IR spectrum of AcBzC$_{11}$-P5N10
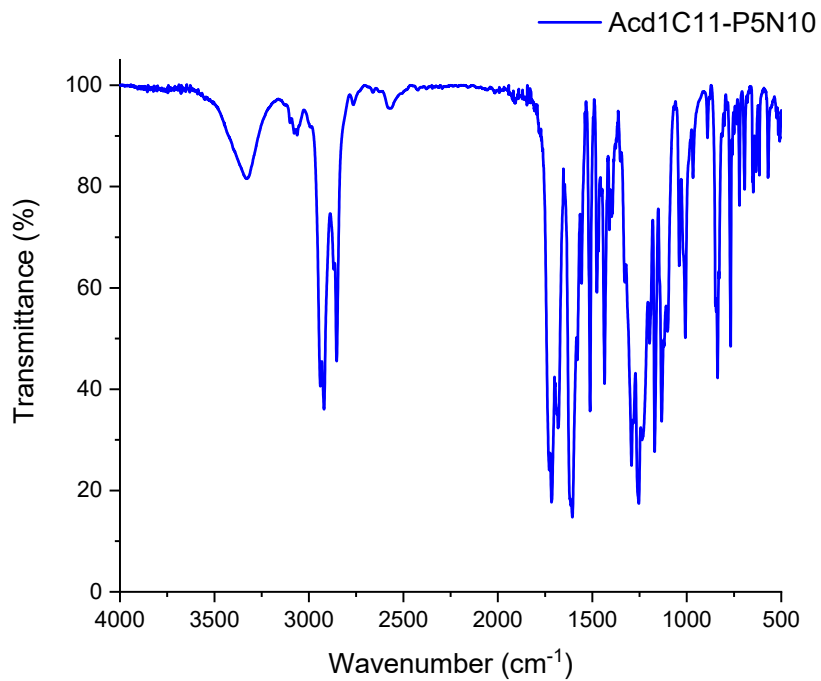
Figure S17. IR spectrum of Acd$_1$C$_{11}$-P5N10
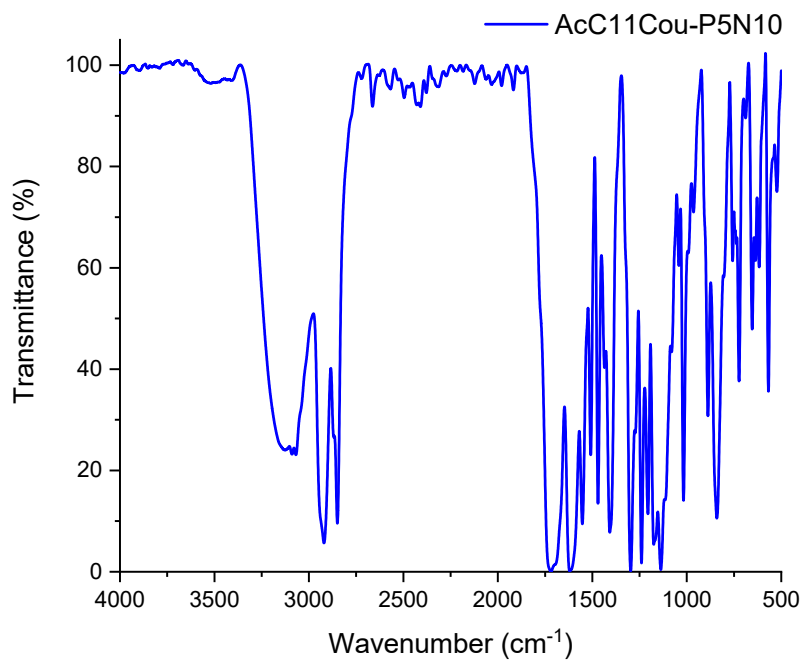
Figure S18. IR spectrum of AcC$_{11}$Cou-P5N10
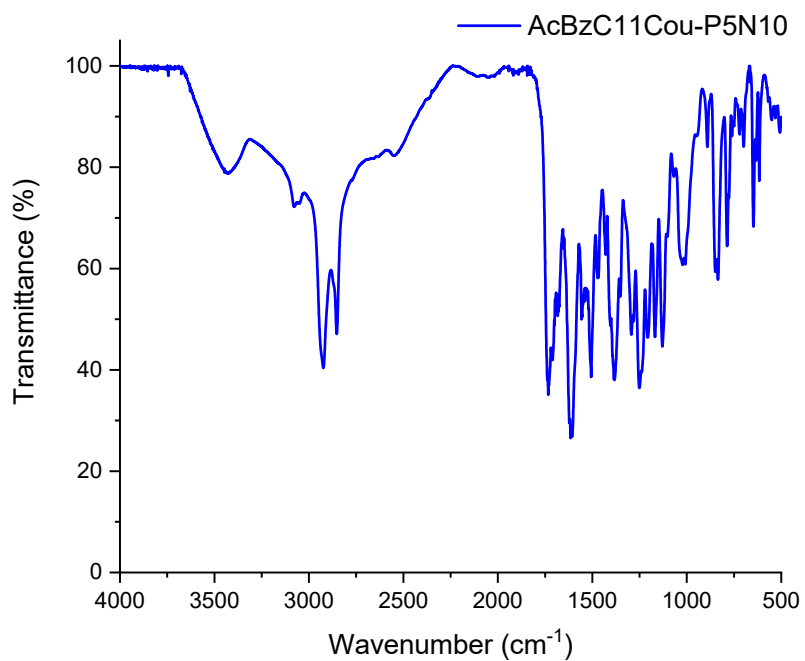
Figure S19. IR spectrum of AcBzC$_{11}$Cou-P5N10
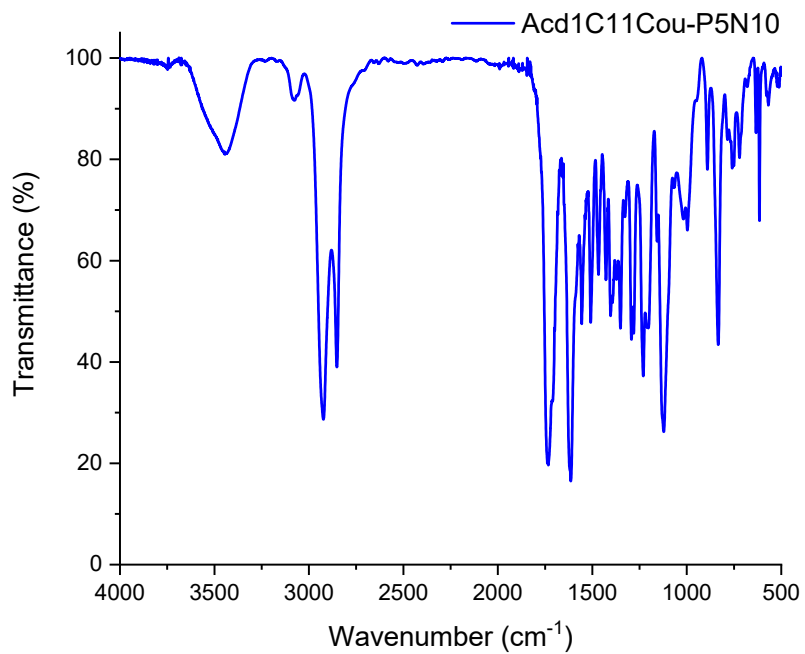
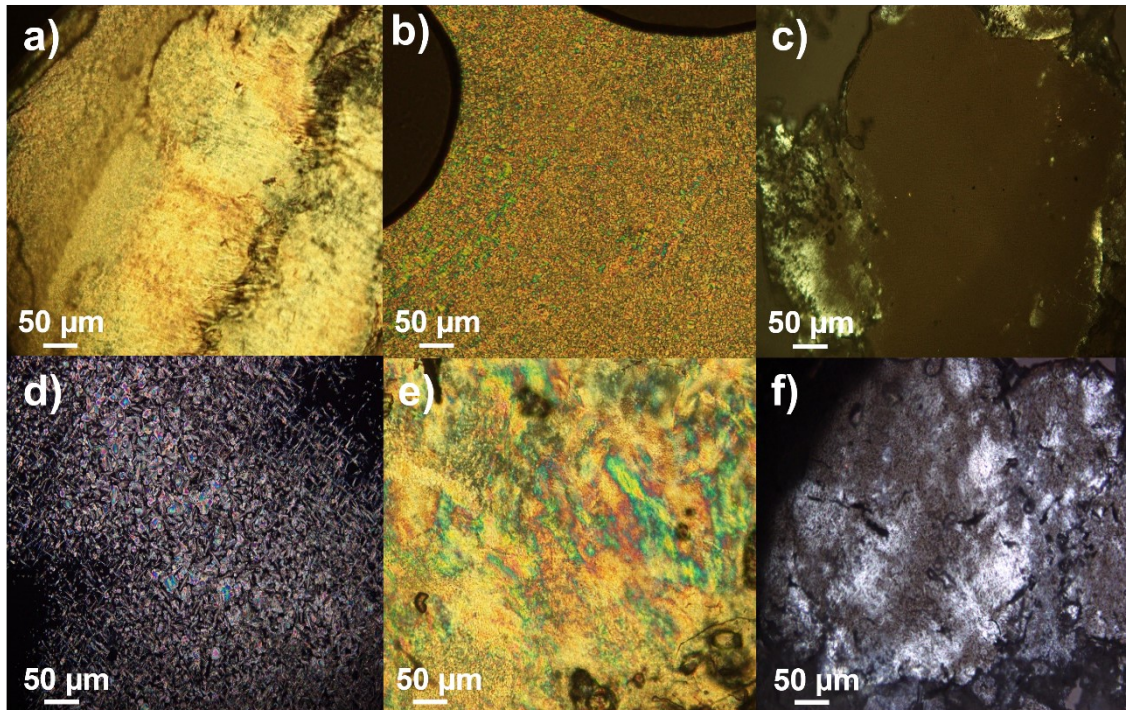*Figure S20. IR spectrum of Acd$_1$C$_{11}$Cou-P5N10*

3.3 POM textures

Figure S21. MOP pictures in the cooling process at room temperature for: a) AcC$_{11}$-P5N10, b) AcBzC$_{11}$-P5N10, c) Acd$_1$C$_{11}$-P5N10, d) AcC$_{11}$Cou-P5N10 e) AcBzC$_{11}$Cou-P5N10 f) Acd$_1$C$_{11}$Cou-P5N10
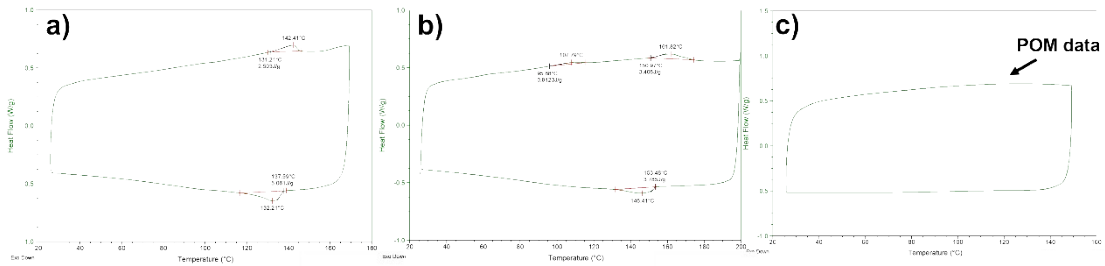
3.4 DSC thermograms

Figure S22. DSC thermograms of a) AcC$_{11}$-P5N10, b) AcBzC$_{11}$-P5N10 and c) Acd$_1$C$_{11}$-P5N10
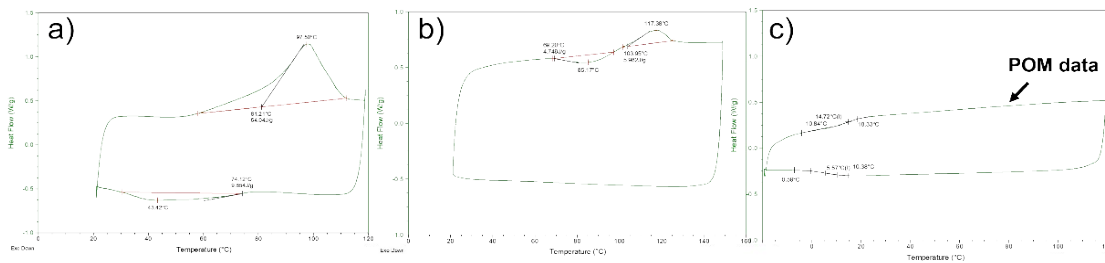

Figure S23. DSC thermograms of a) AcC$_{11}$Cou-P5N10, b) AcBzC$_{11}$Cou-P5N10 and c) Acd$_1$C$_{11}$Cou-P5N10
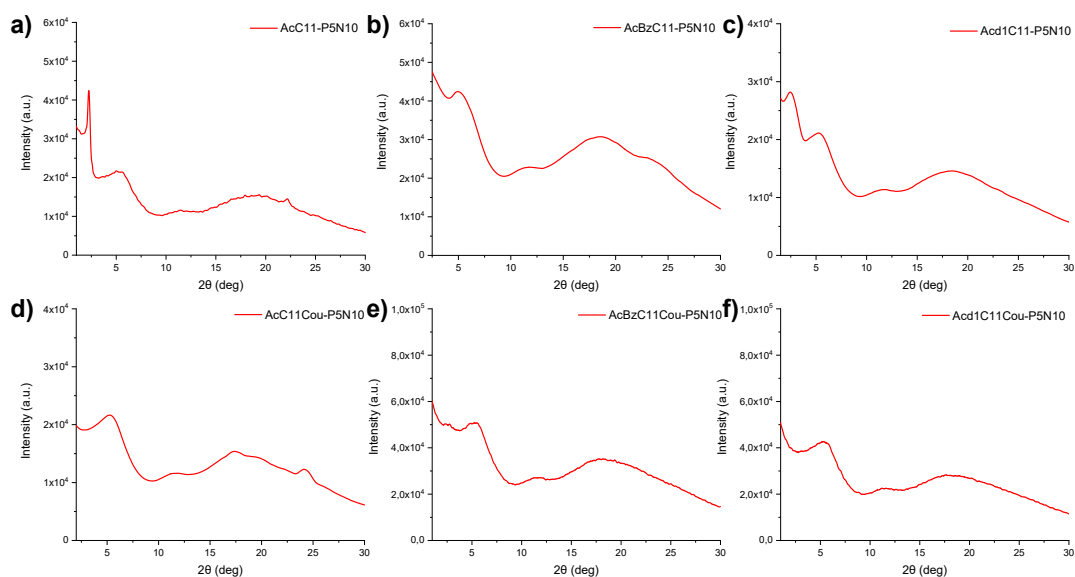
3.5 X-ray diffraction

Figure S24. X-Ray diffractograms of: a) AcC$_{11}$-P5N10, b) AcBzC$_{11}$-P5N10, c) Acd$_1$C$_{11}$-P5N10, d) AcC$_{11}$Cou-P5N10, e) AcBzC$_{11}$Cou-P5N10 and f) Acd$_1$C$_{11}$Cou-P5N10.
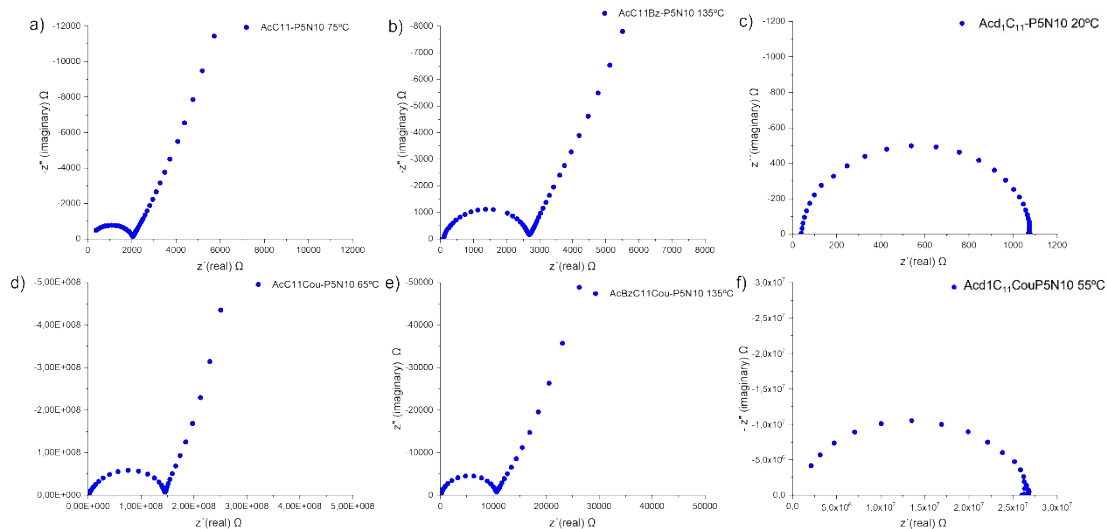
3.6 Nyquist Plots

Figure S25. Nyquist plots of a) AcC$_{11}$-P5N10 at 75ºC, b) AcBzC$_{11}$-P5N10 at 125ºC, c) Acd$_1$C$_{11}$-P5N10 at 20ºC, d) AcC$_{11}$Cou-P5N10 at 120ºC e) AcBzC$_{11}$Cou-P5N10 at 135ºC and f) Acd$_1$C$_{11}$Cou-P5N10 at 55ºC.
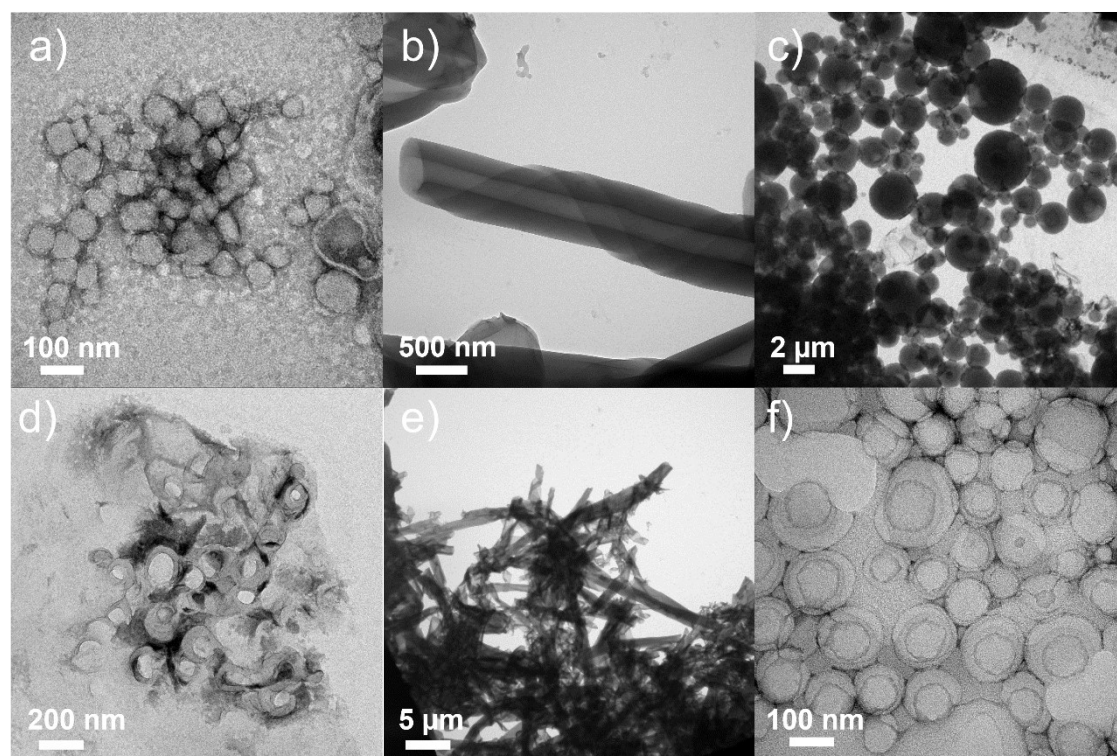
3.7 TEM images

Figure S26. TEM images of AcC$_{11}$Cou-P5N10 a) before d) after photopolymerization, AcBzC$_{11}$Cou-P5N10 b) before e) after photopolymerization and Acd$_1$C$_{11}$Cou-P5N10 c) before f) after photopolymerization.

[i] A. Concellón, M. Marcos, P. Romero, J. L. Serrano, R. Termine and A. Golemme, Angew.Chem.2017,129,1279–1283.

[ii] A. Concellón, T. Liang, A. P. H. J. Schenning, J. L. Serrano, P. Romero and M. Marcos, J. Mater. Chem. C, 2018, 6, 1000--1007

[iii] Y. Sun, F. Zhang, J. Quan, F. Zhu, W. Hong, J. Ma, H. Pang, Y. Sun, D. Tian and H. Li, *Nat Commun* **9**, 2617 (2018).

[iv] R. Martín-Rapún, M. Marcos, A. Omenat, J. Barberá, P. Romero, J. L. Serrano, J. Am. Chem. Soc. 2005, 127, 7397.